Proceedings of the 2005 IEEE
International Conference on Mechatronics
July 10-12, 2005, Taipei, Taiwan

Autonomous Mobile Robot Navigation Using Stereovision

Wei-Song Lin[1], Member, IEEE, Ming-Kang Chuang[2] and Glorious Tien[3]
[1]Department of Electrical Engineering, National Taiwan University, Taiwan ROC, e-mail: weisong@cc.ee.ntu.edu.tw
[2,3]Department of Electrical Engineering, National Taiwan University, Taiwan ROC,
e-mail: r91921054@ntu.edu.tw, r92921055@ntu.edu.tw

***Abstract*- An autonomous mobile robot navigation system based on stereovision perception is developed. The surroundings are recognized by constructing local 3D maps from binocular images. Minimizing the artificial potential energy of the mobile robot on a local 3D map plans a relay position and an approaching path. A self-learning controller using adaptive fuzzy systems is designed to manipulate the dynamic behavior of the mobile robot in tracking a planned path. Using Lagrange formalism, a mathematical model describing the autonomous mobile robot is derived for simulation study. Simulation and experimental results are presented.**

***Index terms*- mobile robot, autonomous navigation, stereovision, adaptive fuzzy control**

I. Introduction

A mobile robot with abilities of environmental exploration and self-learning control can navigate itself autonomously in a dynamical environment. To obtain information about the surroundings for navigation, vision, radar and sonar systems are most frequently adopted as sensors. Stereovision, which functions like human visual perception, can provide not only object detection and recognition but also three-dimensional spatial information of the surroundings. This makes it one of the most potential sensing systems for autonomous mobile robot navigation. Stereovision relies upon a mechanism of stereovision matching to obtain the 3D information. Practically, the information in the intensity value of a single pixel on an image is usually ambiguous for the matching. Therefore, the area-based matching instead of the point-based matching is usually implemented [1], [2], [3]. The matching may transform a pair of stereo images into a disparity map, and finally a 3D map if the focal and baseline lengths are known. For autonomous navigation, an automatic procedure of path planning should be implemented to plan a desired path on the 3D map so that the mobile robot can navigate itself to a destination. Path planning reference to a global 3D map is generally more correct than that using local 3D maps. But, to construct a global 3D map by stereovision needs integrating multiple local 3D maps. This will certainly result in time delay. For quick response of the mobile robot navigation to changes in the environment, our approach is to produce a local 3D map from each stereo image pair. Then, on each local 3D map, a relay position and an approaching path are planned. To compensate lacking of a global map, appropriate motion strategies are designed to direct the robot's visual search.

Successful applications of path planning using the artificial potential field were reported in [4], [5], and [6]. In this paper, the collision-free space on each local 3D map is divided into a collection of cells. Then an artificial potential field is built on these cells. The artificial potential field is the sum of an attractive and a repulsive potential field [7]. Minimizing the artificial potential energy can find a relay position and an approaching path on the local 3D map. Since exploration of an approaching path is restricted in the collision-free cells. Collision avoidance is automatically obtained.

Driving a mobile robot to track a planned path requires steering and dynamic control. However, the mobile robot is a nonholonomic dynamic system with intrinsic non-linearity, un-modeled disturbance and unstructured un-modeled dynamics [8]. This makes the control design a challenge. We equip the mobile robot with a self-learning controller whose parameters are tuned automatically through a learning algorithm instead of specified by the designer. The self-learning controller is composed of two adaptive fuzzy systems to handle the linear and angular velocity control, respectively. A learning mechanism enables the self-learning controller to extract navigating knowledge from experienced data.

II. Kinematics, Dynamics and Self-learning Control of an Autonomous Mobile Robot

Fig. 1 shows a picture of the Autonomous Mobile Robot (AMR) developed in this work.

Fig. 1 A picture of the experimental AMR.

Fig. 2 presents a schematic top view and Fig. 3 illustrates its main components.

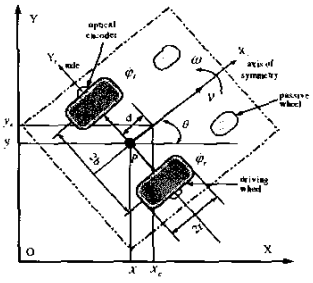

Fig. 2 Schematic top view of the experimental AMR.

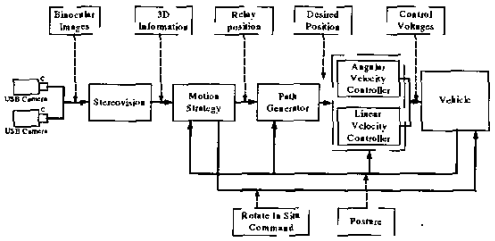

Fig. 3 A block diagram of the AMR.

The system hardware is mainly composed of a motorized vehicle, a stereovision system, a control computer, and batteries. The vehicle has four wheels with two free-to-rotate front wheels and two independent driving rear wheels. Each rear wheel couples with an optical encoder to measure the speed and posture of the AMR. The control computer handles the procedures of stereovision, path planning, and motion control. The stereovision system is a binocular design with two USB CCD cameras as sensors.

A. Kinematics and Dynamics of the AMR

The AMR is known as a nonholonomic dynamic system with intrinsic non-linearity, un-modeled disturbance and unstructured un-modeled dynamics [8]. Autonomous navigation of such a system needs integrated steering and dynamic control. Literature [9], [10], [11] has shown the dynamics of a nonholonomic system with n-dimension generalized coordinates $\mathbf{q} \in \Re^{n\times 1}$ subject to m constraints can generally be described as

$$\mathbf{M}(\mathbf{q})\ddot{\mathbf{q}} + \mathbf{C}(\mathbf{q},\dot{\mathbf{q}})\dot{\mathbf{q}} + \mathbf{F}(\dot{\mathbf{q}}) + \mathbf{G}(\mathbf{q}) + \boldsymbol{\tau}_d = \mathbf{B}(\mathbf{q})\boldsymbol{\tau} + \mathbf{A}^T(\mathbf{q})\boldsymbol{\lambda} \quad (1)$$

and constrained by

$$\mathbf{A}(\mathbf{q})\dot{\mathbf{q}} = 0 \quad (2)$$

where $\mathbf{M}(\mathbf{q}) \in \Re^{n\times n}$ is a symmetric, positive definite inertia matrix, $\mathbf{C}(\mathbf{q},\dot{\mathbf{q}}) \in \Re^{n\times n}$ is the centripetal and Coriolis matrix, $\mathbf{F}(\dot{\mathbf{q}}) \in \Re^{n\times 1}$ denotes the surface friction, $\mathbf{G}(\mathbf{q}) \in \Re^{n\times 1}$ is the gravitational vector, $\boldsymbol{\tau}_d \in \Re^{n\times 1}$ denotes the bounded unknown disturbance including unstructured, un-modeled dynamics, $\mathbf{B}(\mathbf{q}) \in \Re^{n\times r}$ represents the input transformation matrix, $\boldsymbol{\tau} \in \Re^{r\times 1}$ denotes the input vector, $\mathbf{A}(\mathbf{q}) \in \Re^{m\times n}$ is a full rank matrix associated with the constraints, $\boldsymbol{\lambda} \in \Re^{m\times 1}$ is the Lagrange multiplier or the vector of constraint forces. Equation (2) represents the kinematic equality constraints that are independent of time and $\dot{\mathbf{q}}$ must be restricted to the null space of $\mathbf{A}(\mathbf{q})$. Assume $\mathbf{Z}(\mathbf{q}) \in \Re^{n\times(n-m)}$ is a set of smooth linearly independent vector fields spanning the null space of $\mathbf{A}(\mathbf{q})$. Then there exists an auxiliary vector time function $\mathbf{u}(t) \in \Re^{(n-m)\times 1}$, such that for all t

$$\dot{\mathbf{q}} = \mathbf{Z}(\mathbf{q})\mathbf{u}(t) \quad (3)$$

where $\mathbf{u}$ has forms depending on the choices of $\mathbf{Z}(\mathbf{q})$ and not necessarily with any physical significance.

In Fig. 2, an inertial Cartesian frame $\{O, X, Y\}$ and a body frame $\{P, X_c, Y_c\}$ with origin at the middle of the axle of the driving wheels are attached. $\mathbf{p} = [x\ y\ \theta]^T$ denotes a posture vector; b is the half width of the axle of the driving wheels; d is the displacement from the point P along the X_c axis to the center of mass; r is the radius of the driving wheels; m_c is the weight of the body (i.e. excluding the driving wheels and their associated rotors); m_w is the weight of a single driving wheel (i.e. taking the associated rotor into account); I_c is the moment of inertia of the body; I_w is the moment of inertia of each driving wheel about the axle; and I_m is the moment of inertia of each driving wheel about a wheel diameter. We assume the AMR only moves in the direction normal to the axis of the driving wheels (i.e. satisfying the conditions of pure rolling and nonslipping). The constraint of no lateral motion gives

$$\dot{y}\cos\theta - \dot{x}\sin\theta = 0 \quad (4)$$

The constraints of pure rolling and nonslipping at the driving wheels obtain

$$\dot{x}\cos\theta + \dot{y}\sin\theta - b\dot{\theta} = r\dot{\varphi}_l \quad (5)$$

$$\dot{x}\cos\theta + \dot{y}\sin\theta + b\dot{\theta} = r\dot{\varphi}_r \quad (6)$$

The generalized coordinate vector to characterize the AMR can be taken as $\mathbf{q} = [x, y, \theta, \varphi_l, \varphi_r]^T$. The linear velocity v and angular velocity ω in the body frame can be computed as

$$v = \dot{x}\cos\theta + \dot{y}\sin\theta, \text{ and } \omega = \dot{\theta} \quad (7)$$

The relationship between $\dot{\varphi}_l$, $\dot{\varphi}_r$ and v, ω can be obtained by substituting (7) into (5) and (6) as

$$r\dot{\varphi}_l = v - b\omega, \text{ and } r\dot{\varphi}_r = v + b\omega \quad (8)$$

Rewrite (4), (5) and (6) as the following matrix form

$$\mathbf{A}(\mathbf{q}) = \begin{bmatrix} \sin\theta & -\cos\theta & 0 & 0 & 0 \\ \cos\theta & \sin\theta & -b & -r & 0 \\ \cos\theta & \sin\theta & b & 0 & -r \end{bmatrix} \quad (9)$$

Choosing $\mathbf{u} = [v\ \ \omega]^T$ in (3), we obtain

$$\mathbf{Z}(\mathbf{q}) = \begin{bmatrix} \cos\theta & \sin\theta & 0 & \frac{1}{r} & \frac{1}{r} \\ 0 & 0 & 1 & -\frac{b}{r} & \frac{b}{r} \end{bmatrix}^T \quad (10)$$

The Lagrange formalism of the AMR dynamics obtains the following parametric matrices

$$\mathbf{M}(\mathbf{q})=\begin{bmatrix} m & 0 & -m_c d\sin\theta & 0 & 0 \\ 0 & m & m_c d\cos\theta & 0 & 0 \\ -m_c d\sin\theta & m_c d\cos\theta & I & 0 & 0 \\ 0 & 0 & 0 & I_w & 0 \\ 0 & 0 & 0 & 0 & I_w \end{bmatrix},$$

$$\mathbf{C}(\mathbf{q},\dot{\mathbf{q}})=\begin{bmatrix} 0 & 0 & -m_c d\dot{\theta}\cos\theta & 0 & 0 \\ 0 & 0 & -m_c d\dot{\theta}\cos\theta & 0 & 0 \\ 0 & 0 & 0 & 0 & 0 \\ 0 & 0 & 0 & 0 & 0 \\ 0 & 0 & 0 & 0 & 0 \end{bmatrix}, \quad \mathbf{B}(\mathbf{q})=\frac{1}{r}\begin{bmatrix} \cos\theta & \cos\theta \\ \sin\theta & \sin\theta \\ -b & b \\ r & 0 \\ 0 & r \end{bmatrix} \quad (11)$$

The un-modeled dynamics and disturbance are expressed as

$$\mathbf{h}(\mathbf{q},\dot{\mathbf{q}})=\mathbf{F}(\dot{\mathbf{q}})+\mathbf{G}(\mathbf{q})+\boldsymbol{\tau}_d \quad (12)$$

and $\|\mathbf{h}(\mathbf{q},\dot{\mathbf{q}})\|<\varepsilon_h$ is assumed.

B. The Self-learning Controller

Complexity resulted from un-modeled nonlinear dynamics and disturbance makes the AMR controller design a challenge task. Without an accurate mathematical model, conventional feedback or feed-forward linearization approach is usually difficult to obtain an appropriate solution. Therefore, we use as adaptive fuzzy system with self-learning mechanism to construct the controller. The linear and angular velocity is each controlled by an adaptive fuzzy system, which is an extension of Sugeno fuzzy model for the neuro-fuzzy system [12] [13]. Each adaptive fuzzy system has two inputs (x, y), one output z and with a first-order Sugeno fuzzy model. Each fuzzy rule base is composed of if-then rules as,

Rule i

If x is A_i and y is B_i, then $f_i=p_i x+q_i y+r_i$, $i=1,\cdots,N$ (13)

where the consequence parameters are $\boldsymbol{\theta}=[p_1, q_2, r_3,\cdots p_N, q_N, r_N]^T$. Using center-average defuzzification, the overall output of this Sugeno Fuzzy System is obtain as,

$$z=\sum_{i=1}^{N}\overline{w_i}f_i \text{, with } \overline{w_i}=\frac{w_i}{\sum_{j=1}^{N}w_j} \quad (14)$$

where $w_i=\mu_{A_i}(x)\mu_{B_i}(y)$ is a product of memberships. Each membership function is defined as,

$$\mu_j(x)=\frac{1}{1+\left(\frac{x-c_j}{a_j}\right)^{2b_j}} \quad (15)$$

where the premise parameters are $\boldsymbol{\vartheta}=[a_1, b_1, c_1,\cdots,a_{2N}, b_{2N}, c_{2N}]^T$.

Given enough training patterns, the consequence and premise parameters of the adaptive fuzzy system can be determined by a forward training pass followed by a backward training pass [13]. In the forward training pass, the premise parameters are kept unchanged and the consequence parameters are estimated by using the recursive least-squares estimation [14].

Let $\{\mathbf{h}(k), z(k), k=1,2,\cdots,K\}$ be K training patterns with $\mathbf{h}(k)\,\boldsymbol{\theta}=z(k)$, where $\mathbf{h}(k)=[x(k)\ y(k)\ 1]$ and $\theta=\begin{bmatrix} p_1 & p_2\cdots p_N \\ q_1 & q_2\cdots q_N \\ r_1 & r_2\cdots r_N \end{bmatrix}$. Then the recursive least-squares estimation of the consequence parameters is

$$\begin{aligned}\hat{\boldsymbol{\theta}}(k+1)&=\hat{\boldsymbol{\theta}}(k)+\mathbf{P}(k+1)\mathbf{h}^T(k+1)[z(k+1)-\mathbf{h}(k+1)\hat{\boldsymbol{\theta}}(k)]\\ &=\hat{\boldsymbol{\theta}}(k)+\mathbf{P}(k)\mathbf{h}^T(k+1)[\mathbf{I}+\mathbf{h}(k+1)\mathbf{P}(k)\mathbf{h}^T(k+1)]^{-1}\\ &\quad[z(k+1)-\mathbf{h}(k+1)\hat{\boldsymbol{\theta}}(k)]\end{aligned} \quad (16)$$

where $\mathbf{P}(k)=\left[\begin{bmatrix}\mathbf{h}(1)\\ \vdots \\ \mathbf{h}(k)\end{bmatrix}^T\begin{bmatrix}\mathbf{h}(1)\\ \vdots \\ \mathbf{h}(k)\end{bmatrix}\right]^{-1}$. In order to obtain an initial condition, it is necessary to choose an initial value for $k=k_0$ such that $\mathbf{P}(k_0)$ is nonsingular.

In the backward training pass, with the estimated consequence parameters, the error signals propagate backward and the premise parameters are updated by using the back-propagation algorithm [15]. The overall squared error is obtained by

$$E=\sum_{i=1}^{N}E_i=\sum_{i=1}^{N}\frac{1}{2}[d(i)-z(i))^2 \quad (17)$$

where $d(i)$ denotes the desired value. The correction $\Delta\vartheta_i$ applied to the premise parameter $\vartheta_i(k)$ at the kth iteration is defined by the delta rule

$$\Delta\vartheta_i(k)=-\eta\frac{\partial E(k)}{\partial\vartheta_i(k)} \quad (18)$$

where η is the learning rate and $\vartheta_i\in\{a_1, b_1, c_1,\cdots,a_{2N}, b_{2N}, c_{2N}\}$.

In the experimental AMR, the linear and angular velocities are chosen as the training inputs (x, y) of the adaptive fuzzy systems. The corresponding forward and rotation control voltages (1~5 volts) are the desired outputs of the linear and angular velocity controllers, respectively. Each input and output variable is assigned with six membership functions. Therefore, the overall control system has eighteen membership functions for the linear velocity controller (two inputs and one output) and another eighteen membership functions for the angular velocity controller. Each output membership function is a first-order polynomial. Totally, 121 training patterns are collected during manual navigation. Fig. 4 shows these membership functions obtained before and after the training. Fig. 4 (a) and (b) are initial setting of the membership functions for the two input variables (both linear and angular velocity control systems). Fig. 4 (c) and (d) are the trained membership functions of the two input variables of the linear velocity controller. Fig. 4 (e) and (f) are the trained membership functions of the two input variables of the angular velocity controller. The average training errors of the linear and angular velocity controllers are 0.0011501 and 0.0014683, respectively.

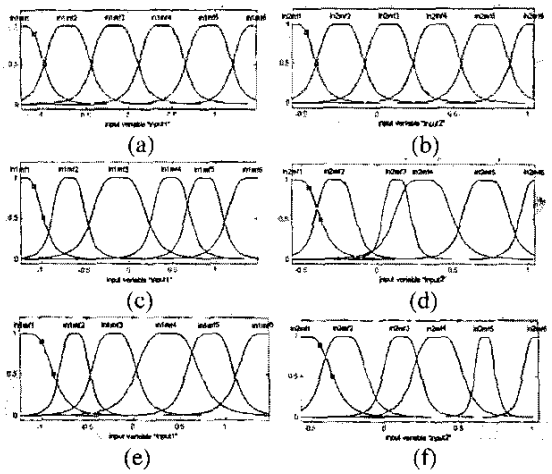

Fig. 4 (a) and (b) initial setting of the membership functions; (c) and (d) the trained membership functions of the linear velocity controller; (e) and (f) the trained membership functions of the angular velocity controller.

III. Autonomous Visual Navigation in Dynamical Environment

A. Constructing Local 3D Maps from Stereo Images

Given a pair of rectified stereo images, stereovision matching tries to find all pairs of correspondences on the conjugate epipolar lines. With these correspondences, a disparity map and then a local 3D map can be constructed. Here, area-based matching, which collects the coherent collections of pixels for stereovision matching is used [1]. The correlation criterion is chosen as

$$C(x,y)= \arg\max_{d} \frac{\sum_{i,j\in W}\left(S_l(x+i+d,y+j)-\bar{S}_l\right)\times\left(S_r(x+i,y+j)-\bar{S}_r\right)}{\sqrt{\sum_{i,j\in W}\left(S_l(x+i+d,y+j)-\bar{S}_l\right)^2}\times\sqrt{\sum_{i,j\in W}\left(S_r(x+i,y+j)-\bar{S}_r\right)^2}} \quad (19)$$

where d represent the disparity, S_r and S_l are the intensity values of the corresponding pixels, W is the comparative window, and x and y are the coordinates. $\bar{S}_r$ and $\bar{S}_l$ denote the average intensity values within the window W. Criterion (19) has the properties of scaling and shift invariance. The disparity between two corresponding points is found by minimizing $C(x, y)$. Large disparity indicates a point close to the camera and vise versa.

Given the focal length and baseline length, a depth value can be calculated from the disparity. Fig. 5 shows the triangular positioning under the ideal epipolar geometry. The world coordinates of a point $P(X,Y,Z)$ are calculated as

$$(X,Y,Z)=\left(\frac{f\,X_l}{Z},\frac{f\,Y_r}{Z},\frac{B\,f}{X_l-X_r}\right) \quad (20)$$

where f is the focal length, B is the baseline length, X_l and X_r are the horizontal image coordinates in metric unit, Y_r is the vertical image coordinate in metric unit.

B. Constructing Artificial Potential Field on a Local 3D Map

The spatial information on a local 3D map allows us to divide the map into free and obstacle cells by using the approximate cell decomposition method [16]. On the free cells, the artificial potential field is established to determine a

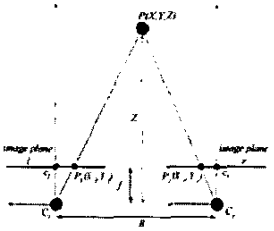

Fig. 5 Relationship between an object point and the image points on the ideal epipolar geometry.

path. The artificial potential field, which measures potential energy by a scalar function, is defined as the sum of an attractive and a repulsive potential field [7]. Obstacles are modeled as emitting a repellant force and the goal position as emitting an attractive force to the robot. When the robot is at the goal position, its potential energy is minimum. In contrary, its potential energy becomes large as closing an obstacle. Since the potential field inclines toward the goal position, following the negative gradient of the potential energy can usually obtain suitable paths. The point of minimal potential is ideally the goal position.

The attractive filed $U_{att}(\mathbf{q})$ should increase as $\mathbf{q}$ moves away from $\mathbf{q}_{goal}$. The function chosen for the attractive field in two-dimensional is a 'parabolic well' form as,

$$U_{att}(\mathbf{q})=\frac{1}{2}C_a\left\|\mathbf{q}-\mathbf{q}_{goal}\right\|=\frac{1}{2}C_a[(x-x_g)^2+(y-y_g)^2] \quad (21)$$

where C_a is a constant of the attractive force, $\mathbf{q}_{goal}=[x_g,y_g]^T$ is the goal position and $\mathbf{q}=[x,y]^T$ represents the interesting point.

The repulsive field $U_{rep}(\mathbf{q})$ should increase as $\mathbf{q}$ moving toward an obstacle. The following piecewise equation is chosen to evaluate the repulsive field:

$$U_{rep}(\mathbf{q})=\begin{cases}\frac{1}{2}\eta\left[\frac{1}{d(\mathbf{q})}-\frac{1}{d_0}\right]^2 & \text{if } d(\mathbf{q})\le d_0\\ 0 & \text{if } d(\mathbf{q})>d_0\end{cases} \quad (22)$$

where $d(\mathbf{q})$ is the current minimum distance between the robot and obstacles, d_0 is the maximum range of the repulsive force, and η is a constant. If $\mathbf{q}$ approaches any obstacles, $U_{rep}(\mathbf{q})$ approaches ∞.

The potential field function is

$$U(\mathbf{q})=U_{att}(\mathbf{q})+U_{rep}(\mathbf{q}) \quad (23)$$

The potential field method of motion planning involves modeling the robot as a point moving under the influence of a potential field that is determined by the set of obstacles and the goal position. Given initial position $\mathbf{q}_{init}$ and goal

position $\mathbf{q}_{goal}$, an algorithm to find a path to approach the goal position by the gradient descent method is

$$\text{Step 1}: \mathbf{q}_{i+1} = \mathbf{q}_i + \delta_i \frac{\vec{\mathbf{F}}(q)}{\left\|\vec{\mathbf{F}}(q)\right\|}, \text{ with } \mathbf{q}_0 = \mathbf{q}_{init} \tag{24}$$

Step 2 : Stop if $\mathbf{q}_{i+1} = \mathbf{q}_{goal}$, otherwise repeats Step 1.

where $\vec{F}(\mathbf{q}) = -\nabla U(\mathbf{q})$ represents the potential force, δ_i is the step size. The step size should be chosen so small that no collision would occur when the robot moves along a straight-line segment between $\mathbf{q}_i$ and $\mathbf{q}_{i+1}$.

When the stereovision does not see the goal position, a relay position $\mathbf{q}_{relay}$ is chosen on the local 3D map by satisfying,

$$\gamma = \underset{\mathbf{q} \in C_{free}}{Max}\left[\frac{d(\mathbf{q})}{1+U_{rep}(\mathbf{q})}\right] \tag{25}$$

The relay position becomes a substitution of the goal position for determining a path in current local 3D map. The evaluation function γ considers both effective exploration of environment and safety. A position far away from the robot and the obstacles is a candidate.

Simulation results of finding a relay position and an approaching path are presented below. A simulated environment is shown in Fig. 6. The region observed by the stereovision is indicated by a triangle. Outside the triangle is seen as obstacles. Using (25), a relay position is found as the peak in Fig. 7 and marked in Fig. 6 as the goal position. Fig. 8 (a) and (b) show the repulsive and attractive fields, respectively. The resultant potential field is presented in Fig. 8 (c). The obstacles have large potential energy and the relay position is the local minimum.

C. Motion Strategies

Four motion strategies are designed to deal with encountering a huge obstacle ahead, avoiding collision, avoiding moving along a passed path, and leaving an entirely searched area.

Strategy 1: A shortcoming of the potential field method is the emergence of local minimum or trap situations (i.e. U-shaped obstacles). Another one is the oscillating behavior in the presence of the obstacles [17]. To avoid these situations, the robot is commanded to rotate *in situ* for a specified angle whenever the distance between the robot and a relay position is too small.

Strategy 2: If a relay position is so close to an obstacle that the next path might oscillate or collide with the obstacle. This relay position is neglected and the robot is commanded to rotate *in situ* for a specified angle to find another relay position.

Strategy 3: Each passed path is seen as a virtual obstacle. The repulsive property of a virtual obstacle is the same as a real one so that a previously passed path will not be repeated.

Strategy 4: If the robot has been successively commanded to rotate *in situ* according to either Strategy 1 or 2 for *M* (specified by designer) times and no suitable relay position is found, next rotation will reverse the direction. A direction reversing cancels all the virtual obstacles and starts a fresh search. Fig. 9 shows the simulation result of searching for an outlet (i.e. goal position) in a maze. Fig. 9 (a) is the maze. The walls are presented as the black areas. The asterisk mark indicates the outlet. The triangle indicates the area observed by the stereovision. The robot must move inside the maze without colliding with the wall. Fig. 9 (b) shows the track of a successful search by applying the motion strategies.

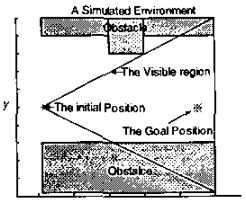

Fig. 6 A simulated environment observed by stereovision.

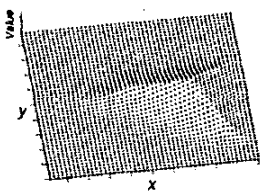

Fig. 7 Evaluation of a relay position.

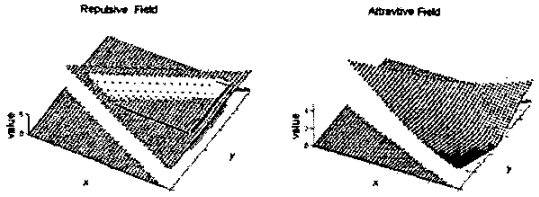

(a) (b)

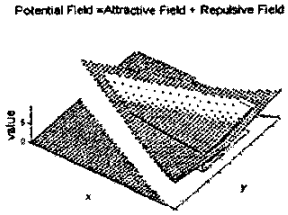

(c)

Fig. 8 (a) The repulsive field, (b) The attractive field, (c) The resultant potential field.

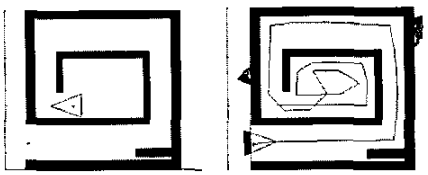

(a) (b)

Fig. 9 Simulation of searching for outlet.

IV. Experimental Results

Pictures in Fig. 10 show consecutive moves of the AMR along a hallway. The linear velocity of the AMR is maintained at 0.2 m/s. Fig. 10 (a) is a rear view of the AMR at the starting point, where the stereovision finds no obstacle

inside the effective view range (2.5m), and decides to go straightforward. During the forward move, a human runs into the hallway and stays beyond the AMR as shown in Fig. 10 (b). The AMR gets a new pair of stereo images at the first relay position. The stereovision finds from the local 3D map that an obstacle, the human, presents. Then, the path planning produces a new path to avoid colliding with the human. Fig. 10 (c) shows the AMR steers itself to bypass the human. Fig. 10 (d) shows the AMR has successfully avoided colliding with the human. Fig. 11 shows the track of the AMR in this experiment. The AMR starts at position (0, 0) and stops at position (3.43, 1.43). The triangles indicate the 3D visible regions. The left triangle represents the first 3D visible region. The right triangle represents the second 3D visible region. Inside the right triangle, an obstacle (gray area) representing the human is found. The resulting posture is 0.05 m at the maximum.

V. CONCLUSION

Main techniques of autonomous mobile robot navigation based upon stereovision guidance have been developed successfully in this paper. Nevertheless, to obtain 3D spatial information efficiently from images captured by un-calibrated stereo cameras is still a challenge. Executing the procedures of image rectification and stereovision matching are time consuming. In the experimental system, the stereovision takes several seconds to complete the construction of a local 3D map. This causes the AMR can only move in a point-by-point manner instead of consecutively. Therefore, efficient method to achieve real-time 3D visual perception should be developed in the future. Motion planning by minimizing the potential energy of the mobile robot has been shown to be reliable. Local minimum traps and some other unfavorable conditions can be avoided by suitably designing the motion strategies. Due to the unknown dynamics and complexity, the control design of the AMR is difficult. The adaptive fuzzy system with self-learning mechanism provides a good solution to this problem. The results from computer simulations and experiments have verified the feasibility of the proposed design.

ACKNOWLEDGEMENT

The financial support for this research from the National Science Council of Taiwan ROC under grant NSC93-2213-E002-106 is gratefully acknowledged.

VI. REFERENCES

[1] O. Faugeras, B. Hotz, H. Mathieu, T. Viville, Z. Zhang, P. Fua, E. Thron, L. Moll, G. Berry, J. Vuillemin, P. Bertin, and C. Proy, "Real time correlation-based stereo: algorithm, implementations and application," *Tech. Rep. 2013, INRIA*, August 1993.

[2] K. Kidono, J. Miura and Y. Shirai, "Autonomous visual navigation of a mobile robot using a human-guided experience," *Robotics and Autonomous Systems*, vol. 40, nos. 2-3, pp. 124-132, 2002.

[3] H. Koyasu, J. Miura, and Y. Shirai, "Mobile robot navigation in dynamic environments using omnidirectional stereo," in *Proceedings of the IEEE International Conference on Robotics & Automation*, pp. 14-19, 2003.

[7] O. Khatib, "Real-time obstacle avoidance for manipulators and mobile robots," *The International Journal of Robotics Research*, vol. 5, no. 1, Spring, 1985.

[4] D.C. Conner, A. Rizzi, and H. Choset, "Composition of local potential functions for global robot control and navigation," in *Proceedings of 2003 IEEE/RSJ International Conference on Intelligent Robots and Systems* (IROS 2003), vol. 4, pp. 3546- 3551, October 2003.

[5] S.A. Masoud and A.A. Masoud, "Constrained motion control using vector potential fields," *IEEE Transactionon Systema, Man and Cybernetics-Part A*, vol. 30, no. 3, pp. 251-272, May 2000.

[6] M. Mohan, D. Busquets, R. López de Mántaras, C. Sierra; *Integrating a Potential Field Based Pilot into a Multiagent Navigation Architecture for Autonomous Robots*. IIIA Technical Report TR-2004-02.

[8] D.T. Greenwood, *Principles of Dynamics*, Prentice-Hall, 1988.

[9] P.S. Tsai, T.F. Wu, F.R. Chang and L.S. Wang, "Tracking Control of Nonholonomic Mobile Robot Using Hybrid Structure," *The 6th World Multiconference on Systemics, Cybernetics and Informatics*, Orlando, Florida, 2002.

[10] X. Yun, and Y. Yamamoto, "Internal Dynamics of a Wheeled Mobile Robot," in *Proceeding of the IEEE/RSJ International Conference on Intelligent Robots and Systems*, pp.1288-1293, 1993.

[11] F.L. Lewis, C.T. Abdallah, and D.M. Dawson, *Control of Robot Manipulators*, New York: MacMillan, 1993.

[12] T. Takagi and M. Sugeno, "Fuzzy identification of systems and its applications to modeling and control," *IEEE Transactions on Systems, Man, and Cybernetics*, vol. SMC-15, no. 1, pp. 116-132, 1985.

[13] J-S Jang, "ANFIS: adaptive-network-based fuzzy inference systems," *IEEE Transactions on Systems, Man, and Cybernetics*, vol. 23, no. 3, pp. 665-685, May 1993.

[14] K.J. Åström and Björn Wittenmark, *Computer Controlled Systems: Theory and Design*, Prentice-Hall, Inc., Englewood Cliffs, N.J., p.328-335, 1984.

[15] S. Haykin, *Neural Networks: A Comprehensive Foundation*, Prentice Hall International, Inc. p.161-175, 1999.

[16] J.C. Latombe, *Robot Motion Planning*, Kluwer Academic Publishers, Boston, MA., 1991.

[17] Y. Koren and J. Borenstein, "Potential field methods and their inherent limitations for mobile robot navigation," in *Proceedings of the IEEE Conference on Robotics and Automation*, Sacramento, California, pp. 1398-1404, 1991.

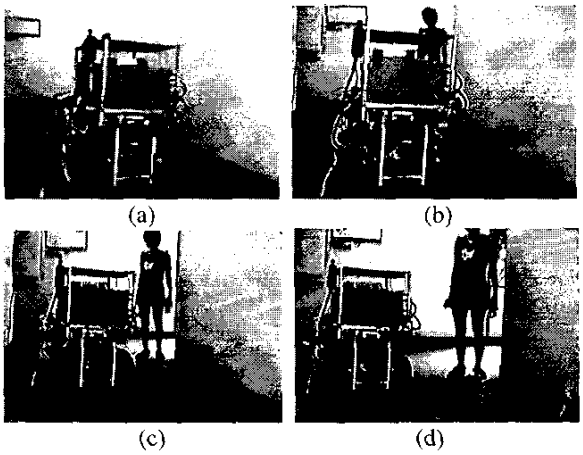

Fig. 10 Consecutive moves of the AMR along a hallway.

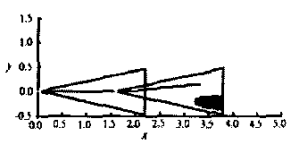

Fig. 11 Moving path of the AMR.